旁路分流 MIG 电弧熔钎焊接镁/钢异种金属接头特性

苗玉刚， 吴斌涛， 韩端锋， 徐向方*
（哈尔滨工程大学 船舶工程学院，哈尔滨 150001）

摘 要： 以 AZ31 镁合金与 Q235 镀锌钢板为研究对象，进行旁路分流 MIG 电弧熔钎焊接工艺试验，在获得稳定可靠的焊接过程和美观的焊缝成形的同时，实现了镁/钢异种金属的可靠连接. 同时采用金相显微镜，高速摄像机和拉伸试验机对焊接接头的组织、熔滴过渡过程以及力学性能进行观察与分析. 结果表明，焊接过程中熔滴的排斥过渡增加了熔滴过渡的时间，使得熔滴润湿铺展更为均匀，且保证了界面层元素的充分结合. 拉伸试验表明，焊接接头的抗拉强度达 133 MPa，约为母材强度的 70%，接头断裂发生在镁合金焊缝处，呈韧性断裂的形貌特征.

关键词： 镁合金； 镀锌钢； 旁路分流 MIG 电弧熔钎焊； 熔滴过渡； 焊接特性
中图分类号： TG402 **文献标识码：** A **文章编号：** 0253－360X(2014)01－0025－04

0 序 言

镁及镁合金是目前工业中应用最有前景的有色金属结构材料之一，钢是工业生产中应用最广泛的一种金属. 由于镁合金与钢应用的广泛性和交叉性，将镁/钢连接形成复合结构，既可兼顾整体减重，又可增强局部承载，在汽车、航天航空、船舶等领域具有巨大的应用潜力[1,2]. 由于镁、钢之间溶解度小，熔点差异大，相互之间很难发生冶金反应，传统熔焊方法很难实现钢/镁的有效连接. 尽管点焊[3]、搅拌摩擦焊[4]、夹镍层激光电弧复合焊[5]等方法实现了镁/钢异种金属的连接，但这些方法易受工件形状和尺寸的限制，且效率低，难以满足大批量生产的需求. Tan 等人[6]采用激光熔钎焊的方法实现了镁/钢的可靠连接，但焊接成本明显增加.

旁路分流 MIG 电弧熔钎焊方法由于具有热输入低、电弧稳定性好、焊接成本低等特点，可应用于铝/钢、镁/钢等异种金属材料的连接. 文中以 AZ31 镁合金和 Q235 镀锌钢板为研究对象，系统研究了旁路分流 MIG 电弧熔钎焊的工艺特性及其熔滴过渡的变化过程，并对该工艺的焊缝成形、接头形貌和力学性能等问题进行研究. 研究结果将为深刻理解镁/钢异种金属旁路分流 MIG 电弧熔钎焊过程提供试验数据和理论支持，并为该项技术的工程应用提供技术依据.

1 试验方法

试验材料分别为 2 mm 厚的 Q235 镀锌钢板和 2.5 mm 厚的 AZ31 镁合金板. 其化学成分如表 1 和表 2 所示. 焊接时，采用与母材同质的 AZ31 镁合金焊丝作为填充材料，焊丝直径为 1.6 mm.

表 1 Q235 镀锌钢的化学成分(质量分数，%)
Table 1 Chemical compositions of Q235 galvanized steel

C	Si	Mn	P	S	Fe
0.14～0.22	≤0.30	0.30～0.65	≤0.045	≤0.050	余量

表 2 AZ31 镁合金的化学成分(质量分数，%)
Table 2 Chemical compositions of AZ31 magnesium alloy

Mg	Si	Mn	Cu	Zn	Ti	Fe	Al
0.8～6.8	≤0.40	0.5～0.8	≤0.10	≤0.20	0.02～0.1	0～0.04	余量

利用自制的旁路分流 MIG 电弧焊接设备进行工艺试验，其工艺机理见图 1. 焊接时，在 MIG 焊枪一侧施加旁路钨极焊枪进行分流，这样焊接时流经 MIG 焊主弧的电流 I 被分成两部分：一部分经由旁路流回焊接电源 I_p，另一部分为施加到母材上的电

收稿日期：2013－08－10
基金项目：国家自然科学基金资助项目(51005049)
* 参加此项研究工作的还有李小旭

流 I_m. 在焊接过程中,IGBT 控制系统通过改变旁路电阻就可以调节旁路电流 I_p,进而可调节施加到母材上的电流 I_m,使得作用于熔池和熔滴上的热、力处于理想水平,是一种高效、可控的焊接方法.

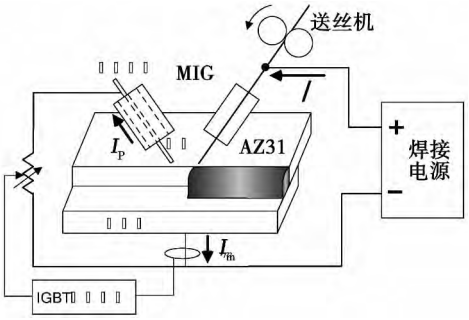

图 1 旁路分流 MIG 电弧熔钎焊工艺机理示意图

Fig. 1 Sketch for bypass-current MIG welding-brazing

在试验过程中,主路 MIG 焊接电流为 76 A、电弧电压为 19 V,旁路分流值为 20 A,焊接速度为 53 cm/min,旁路钨极距母材高度为 1 mm,钨极与焊丝间距为 3 mm,MIG 焊枪距母材高度为 6 mm,MIG 焊枪保护气体流量为 15 L/min,旁路焊枪保护气体流量为 5 L/min.

2 试验结果及分析

2.1 焊缝成形

图 2 为镁/钢旁路分流 MIG 电弧熔钎焊的焊缝成形. 可以看出,该工艺可获得表面成形光滑、均匀美观的焊缝. 分析认为,旁路电弧的存在不仅可分流一部分流经母材的焊接电流,还可使 MIG 焊枪的主电弧变得更加稳定,并且明显减少焊接飞溅. 另外,旁路与主路形成的耦合电弧在熔化焊丝的同时可对镀锌钢板进行预热,导致熔融的液态钎料在钢母材上的润湿铺展更加均匀,焊缝成形更为美观.

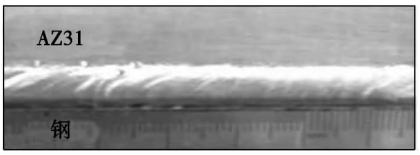

图 2 镁/钢接头焊缝成形

Fig. 2 Seam of bypass-current MIG welding-brazed Mg/Fe

2.2 接头形貌

图 3 为镁/钢旁路分流 MIG 电弧熔钎焊的接头横截面形貌. 由图 3a 可以看出,搭接接头上侧的镁合金为熔焊结合,即低熔点 AZ31 镁母材局部熔化,与液态填充钎料混合后凝固形成焊缝,且存在明显的熔合区;而搭接接头下侧的镀锌钢为钎焊结合,即高熔点的钢母材不发生熔化,通过液态镁合金钎料在镀锌钢上的润湿和铺展作用形成钎焊连接,呈典型熔焊—钎焊的接头形貌.

从图 3b 还可以看出,在镁/钢异种金属界面处结合良好,且形成的界面层很薄,这与焊接电弧对母材的热输入较低有关.

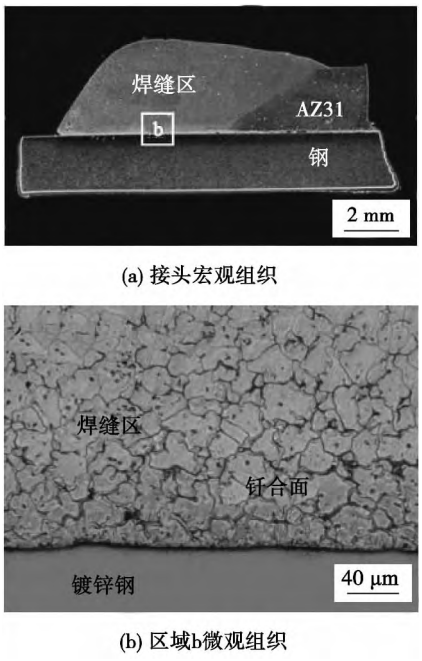

(a) 接头宏观组织

(b) 区域b微观组织

图 3 镁/钢异种金属接头形貌

Fig. 3 Joint morphology of bypass-current MIG welding-brazed Mg/steel

分析认为,该焊接电弧的加热区主要集中在镁合金上,会导致低熔点的镁合金局部熔化,与液态钎料混合后形成焊缝区;在镀锌钢侧,焊接电弧作用在钢母材上的热输入较低,加之钢的熔点较高,未见熔化现象,熔融的液态钎料在镀锌钢板表面润湿和铺展,并与钢表面的镀锌层形成一层钎合面. 相关试验表明,该钎合面的结合情况是保证镁/钢异种金属接头性能的关键所在.

2.3 熔滴过渡

图 4 为镁/钢旁路分流 MIG 电弧熔钎焊的熔滴过渡过程. 由图 4 中可以看出,由于旁路电弧的存在,使得焊接过程的稳定性增加,焊接飞溅明显较少或几乎无飞溅. 熔滴过渡较为平稳,当熔滴下落时,明显为向上排斥,呈典型的排斥过渡. 由于熔滴的排斥过渡,使得熔滴润湿铺展面积变大,滴落过程的

平稳，使得焊缝成形更为均匀，因此形成高质量焊缝.

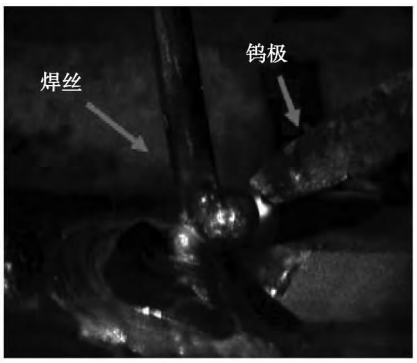

(a) 熔滴形成阶段

(b) 熔滴排斥阶段

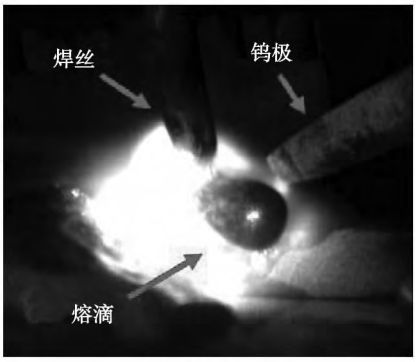

(c) 熔滴下落阶段

图 4　熔滴过渡的不同阶段

Fig. 4　Different process of droplet transfer

分析认为，旁路电弧的产生不仅稳定了主路 MIG 焊电弧，还扩展了耦合电弧的弧根，并包围整个熔滴，从而使得作用于熔滴上的电磁力方向驱使熔滴的过渡. 旁路电弧会对从熔滴上方流向下方的等离子气流产生加速作用，从而促使等离子流力变大，有利于熔滴脱离焊丝，使熔滴过渡平稳.

此外，由于耦合电弧等离子体和熔滴具有良好的导电性能，必然导致主弧的熔滴过渡机制(包括熔滴过渡类型、临界电流阈值以及熔滴冲击力等)与常规 MIG 焊的有很大不同，另见文献[7]专述. 由于旁路耦合 MIG 焊电弧产生的斑点力与镁合金元素的大量蒸发产生的金属蒸气对熔滴产生的反作用力使得整个焊接过程的熔滴过渡为排斥过渡. 排斥过渡延长了熔滴下落的时间，以此便增加了元素之间的融合，使得镁母材、填充钎料以及锌层充分熔融和铺展，形成了均匀美观的焊缝.

2.4　力学性能

利用型号为 Zwick/Roell Z010 的电子万能材料拉伸试验机进行镁/钢异种金属熔钎焊接头拉伸试验，拉伸速度为 2 mm/min. 拉伸试样采用非标准光滑试样，数据点为每秒 10 个点，温度 20 ℃. 图 5 为镁/钢接头的拉伸位移—抗拉强度曲线. 图 6 为拉伸试样的断裂位置.

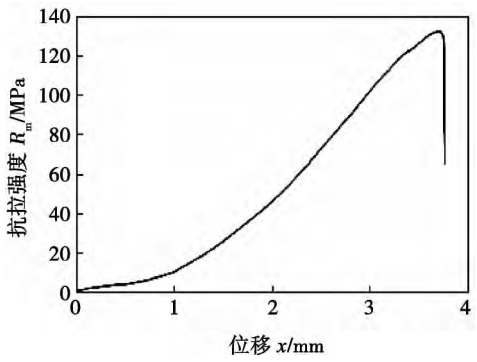

图 5　镁/钢接头的拉伸位移—抗拉强度曲线

Fig. 5　Relation between tensile displacement and strength of Mg/steel joint

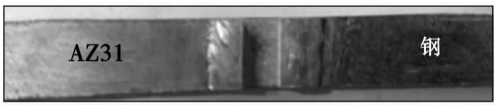

图 6　拉伸试样的断裂位置

Fig. 6　Fracture location of tensile test

从图 5 可以看出，镁/钢旁路分流 MIG 电弧熔钎焊接头的抗拉强度可达 133 MPa，约为母材抗拉强度(191.6 MPa)的 70 %. 从图 6 可以看出，拉伸试样的断裂位置发生在镁合金焊缝上，而非钎合面处，拉伸断面平整光滑，断口颜色灰暗.

从图 5 和图 6 还可以看出，断裂前接头试样有一定的拉伸位移，且在断裂前拉伸试样发生了一定的颈缩，这说明旁路分流 MIG 电弧钎焊接头具有良好的塑性和较高的抗拉强度.

2.5　断口分析

图 7 为镁/钢旁路分流 MIG 电弧熔钎焊接头断口形貌. 图 7a 为钎焊接头的宏观形貌. 图 7b 为图 7a 中 A 区域微观形貌. 可以看出，接头的断口表面粗糙不平，且断口表面分布很多韧窝，为典型韧性断

裂的形貌特征.

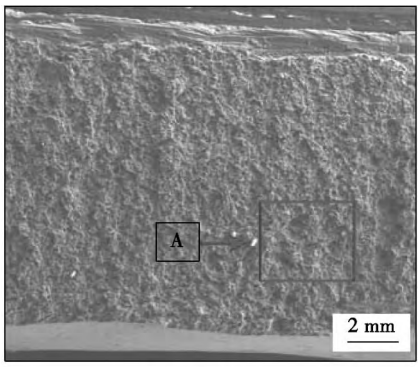

(a) 宏观形貌

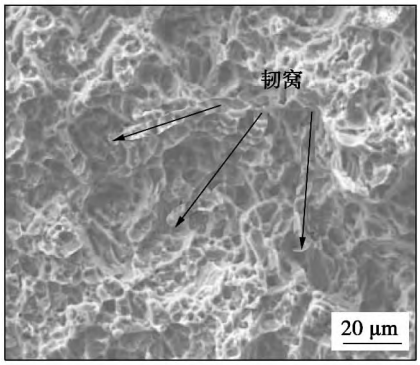

(b) 图7a中A区域微观形貌

图 7 镁/钢接头断口形貌

Fig. 7 Fracture morphology of Mg/steel joint

3 结 论

(1) 采用旁路分流 MIG 电弧熔钎焊的方法,获得了具有熔焊和钎焊双重性质的接头,且镁/钢异种金属界面处结合良好,形成的钎合面很薄,这与焊接电弧对母材的热输入较低有关.

(2) 焊接过程中旁路电弧的存在加速了熔滴脱离焊丝,熔滴过渡过程更为稳定. 此外,熔滴的排斥过渡增加了熔滴下落的时间,使得熔滴润湿铺展更为均匀,使得液态镁合金、填充钎料在镀锌钢板上充分润湿铺展,形成了均匀美观的焊缝.

(3) 镁/钢旁路分流 MIG 电弧熔钎焊接头的抗拉强度可达 133 MPa,约为母材抗拉强度(191.6 MPa)的 70%,接头断裂发生在镁合金焊缝处,且断口表面粗糙不平分布着很多韧窝,呈典型韧性断裂的形貌特征.

参考文献:

[1] Goken J, Bohlen J, Hort N, *et al*. New development in magnesium technology for light weight structures in transportation industries [J]. Materials Science Forum, 2003: 426/432(1): 153 – 160.

[2] Campbell F C. Manufacturing technology for aerospace structural materials [M]. 1st ed. UK: Elsevier Ltd., 2006.

[3] 陈益平, 邵景辉, 胡德安, 等. 镁/钢异种材料点焊接头力学性能及显微组织分析 [J]. 焊接学报, 2013, 34(4): 101 – 104.
Chen Yiping, Shao Jinghui, Hu Dean, *et al*. Analysis of microstructure and mechanical properties of dissimilar metal spot welded joint between magnesium alloy and steel [J]. Transactions of the China Welding Institution, 2013, 34(4): 101 – 104.

[4] 黄勇兵, 李建萍, 黄春平, 等. 镁和钢搅拌摩擦焊接头组织分析 [J]. 焊接学报, 2013, 34(5): 67 – 70.
Huang Yongbing, Li Jianping, Huang Chunping, *et al*. Microstructure of friction stir welded joint of magnesium and steel [J]. Transactions of the China Welding Institution, 2013, 34(5): 67 – 70.

[5] 单 闯, 宋 刚, 刘黎明. 激光 – TIG 复合热源焊接参数对镁/钢异种材料焊接接头的影响 [J]. 焊接学报, 2008, 29(6): 57 – 60.
Shan Chuang, Song Gang, Liu Liming. Effect of laser-TIG hybrid welding parameters on joint of Mg to steel [J]. Transactions of the China Welding Institution, 2008, 29(6): 57 – 60.

[6] Tan Caiwang, Li Liqun, Chen Yanbin, *et al*. Laser-tungsten inert gas hybrid welding of dissimilar metals AZ31B Mg alloysto Zn coated steel [J]. Material and Design, 2013, 49(2): 766 – 773.

[7] 卢立晖. 铝 – 钢异种金属脉冲旁路耦合电弧 MIG 熔钎焊方法及机理研究 [D]. 兰州: 兰州理工大学, 2012.

作者简介: 苗玉刚,男,1978 年出生,博士,副教授,硕士研究生导师. 主要从事船舶与海洋工程焊接工艺及数值模拟方面的教学和科研工作. 发表论文 20 余篇. Email: miaoyg@ hrbeu. edu. cn

China). pp 17 – 20

Abstract: To improve the stability of welding technology and reduce the post-weld repair due to defects like surface imperfections in key steel structure, a new method by applying auxiliary electric field between the slag and metal during submerged arc welding to guide electric current was developed. The electric signal instrument was used to collect arc voltages for statistics and analysis. The results show that the electric conductivity of molten slag can be improved with tungsten electrode as the cathode, and the electrons are guided into the arc centre to contract the welding arc. Meanwhile, positive and negative ions in the molten slag and weld pool metal migrated to the interface and combined into active oxides with low surface energy. Thus the wetting and spreading performance of molten slag on the surface of weld pool metal are improved. With the beneficial effect brought by the auxiliary electric field, the weld surface is smooth, the appearance of weld and especially the consistency of weld width are improved. Also, the welding process is more stable.

Key words: auxiliary electric field; submerged arc welding; welding processing; arc stability

Ultrasonic phased array inspection technology for defects in friction stir welded seam YU Liang, CHEN Yuhua, HUANG Chunping, GE Junwei, KE Liming (School of Aeronautical Manufacturing Engineering, Nanchang Hangkong University, Nanchang 330063, China). pp 21 – 24

Abstract: Ultrasonic phased array inspection technology was used to detect the defects in friction stir welded seam with different thicknesss. The inner defects were precisely quantified and represented by changing the scanning angle, focus depth and focus size of phased array. The morphology of the defects was observed by dissecting the welded seam with defect signal. The results show that the inner defects can be quickly determined with higher detection sensitivity probe. The position, size and distribution of the defects can be precisely detected through three views obtained by different scanning modes. The shape and peak value of echo signal were determined by the defect shape. The echo signal of little hole defect was a sharp peak and the peak value was large. The echo signals of aluminium coating and loose defects were multiple-cluster wave. In S-scan, the lightspots of loose defect were more intensive and distributed more widely than aluminium coating defect.

Key words: aluminium alloy; friction stir welding; ultrasonic phased array; weld defect

Joint characteristics of magnesium/steel dissimilar metals during bypass-current MIG welding-brazing MIAO Yugang, WU Bintao, HAN Duanfeng, XU Xiangfang, LI Xiaoxu (College of Shipbuilding Engineering, Harbin Engineering University, Harbin 150001, China). pp 25 – 28

Abstract: Bypass-current MIG welding-brazing of AZ31 magnesium alloy and Q235 galvanized steel was carried out. The results show that the technology could obtain stable welding process and good bead appearance. The optical microscopy, high-speed cameras and tensile testing machine were applied to observe and analyze the joint morphology, droplet transfer process and mechanical properties. It was found that the repelled transfer of droplet in the welding process prolonged the droplet transfer time, resulting in more uniformly wetting and spreading of droplet and integration of alloying elements in the interface. The tensile strength reached 133 MPa, about 70% of the base material. The joint fracture occurred in the magnesium weld, displaying ductile fracture features.

Key words: magnesium alloy; galvanized steel; bypass-current MIG welding-brazing; droplet transfer; welding characteristic

Effect of aging treatment on interfacial microstructure and mechanical properties of Sn-Zn-Ga-Nd soldered joints XUE Peng, XUE Songbai, SHEN Yifu (College of Materials Science and Technology, Nanjing University of Aeronautics and Astronautics, Nanjing 210016, China). pp 29 – 32

Abstract: The effect of aging treatment at 150 ℃ for different time on the interfacial microstructure and mechanical properties of Sn-Zn-Ga-Nd soldered joints was investigated. The results show that Ga could suppress the formation of Sn-Nd compound during the aging process and improve the reliability of soldered joints. The mechanical properties of the soldered joints further increased with the addition of Ga and Nd. The shear strength of soldered joints with Sn-Zn-Ga-0.08Nd decreased with increasing aging time, but was still remarkably higher than that of as-soldered joint with Sn-Zn solder.

Key words: aging treatment; soldered joint; interface; shear strength

Quality assessment using dynamic voltage characteristics in small scale resistance spot welding of titanium alloy ZHAO Dawei[1], WANG Xinyang[2], WANG Yuanxun[1], YANG Hao[1], ZHANG Lei[1] (1. Hubei Key Lab for Engineering Structural Analysis and Safety Assessment, Huazhong University of Science and Technology, Wuhan 430074, China; 2. Nanjing Kisen International Engineering Co., Ltd, Nanjing 210036, China). pp 33 – 36

Abstract: The voltage between the electrodes in small-scale resistance spot welding (SSRSW) of titanium alloy was collected by data acquisition system. The experiments revealed that the dynamic voltage signal included a lot of welding quality information. In order to demonstrate this finding and monitor the welding quality, the back-propagation artificial neural network (ANN) was employed to forecast the nugget diameter. The maximum predicted error of ANN was about 6.5%. Adjusting and monitoring the voltage waveform could be used to forecast the formation of weld nugget and monitor the quality of welded joints.

Key words: small-scale resistance spot welding; voltage waveform; quality monitoring; artificial neural network

Microstructure and mechanical properties of 5083 aluminum alloy joint by TIG welding CHEN Cheng[1], XUE Songbai[1], SUN Huhao[1], LIN Zhongqiang[2], LI Yang[1] (1. College of Materials Science and Technology, Nanjing University of Aeronautics and Astronautics, Nanjing 210016, China; 2. Zhejiang Yuguang Aluminum Material Co., Ltd, Wuyi 321200, China).